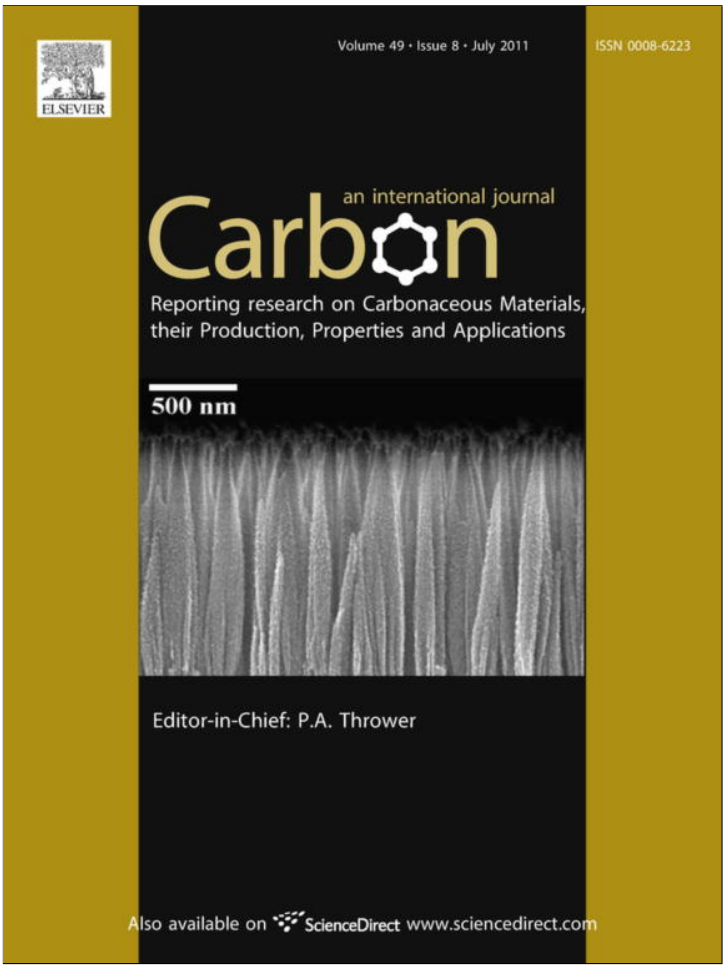

CARBON 49 (2011) 2809–2816

available at www.sciencedirect.com

ScienceDirect

journal homepage: www.elsevier.com/locate/carbon

High-quality few layer graphene produced by electrochemical intercalation and microwave-assisted expansion of graphite

Gustavo M. Morales [a,*], Pablo Schifani [a], Gary Ellis [b], Carmen Ballesteros [c], Gerardo Martínez [b], César Barbero [a], Horacio J. Salavagione [b,*]

[a] Universidad Nacional de Río Cuarto (UNRC), Departamento de Química, Ruta 36, Km 601, 5800 Río Cuarto, Argentina
[b] Instituto de Ciencia y Tecnología de Polímeros (ICTP-CSIC), C/Juan de la Cierva 3, 28006 Madrid, Spain
[c] Universidad Carlos III de Madrid, Departamento de Física, Avenida Universidad 30, 28911 Leganés, Spain

ARTICLE INFO

Article history:
Received 28 December 2010
Accepted 2 March 2011
Available online 6 March 2011

ABSTRACT

Few-layer graphene is synthesized from electrochemically-produced graphite intercalation compounds in aqueous perchloric acid. Although anodic intercalation is more efficient in terms of time, cathodic pre-treatment is preferred to avoid the formation of graphite oxide. The materials are characterized by high resolution transmission electron microscopy and scanning electron microscopy, UV–visible, infrared and Raman spectroscopy. We demonstrate that the method, under the experimental conditions used in this work, does not produce damage to the sp^2 carbon lattice. The synthetic approach using electrochemical-potential control is very promising to obtain, in a controllable manner, graphene with different degrees of oxidation.

1. Introduction

Graphene, a one-atom-thick planar sheet of sp^2-bonded carbon atoms, is a quasi-2-dimensional (2D) material. The fascinating properties of single-layer graphene (SLG) and few-layer graphene (FLG) have made it one of the most promising materials of the first decade of the 21st century [1]. It has been observed that graphene presents an ambipolar field effect [2], a quantum Hall effect at room temperature [3–5], very high charge carrier mobility that is temperature-independent and translates into ballistic transport [6,7], and very high surface area [8]. Graphene and its derivatives are promising candidates as components for applications in the field of energy-storage and energy conversion materials, thermally and electrically conductive reinforced nanocomposites, nanoelectronics and sensors, among many others.

However, graphene suffers from a problem which is common to many novel nanomaterials; the lack of effective methods for large-scale production. Consequently, full exploitation of the properties of graphene still requires the development of methods to produce large quantities of FLG with low density of defects in the crystal lattice [9]. The exfoliation of expandable graphite (EG) via graphite intercalation compounds (GIC) may be one of the most attractive methods proposed because this process, which has been extensively studied in the past, is cheap and scalable [10,11]. Nevertheless, the possibility of its use as a route to obtain FLG without damage to the sp^2 structure – denominated as high quality graphene, HQG – is still not clear. Stankovich et al. [12] reported numerous failed attempts to produce HQG from GIC, including the synthesis by exfoliation of potassium-intercalated graphite [13].

Recently, electrochemical techniques have been employed in the production of graphene. Guo et al. reported the electrochemical reduction of exfoliated graphite oxide (GO) in PBS [14] and sodium sulfate [15] solutions. However, this method presents the same disadvantages as all synthetic approaches where GO is used as starting material; the sp^3 defects cannot be efficiently transformed back to sp^2 as was evident from

* *Corresponding authors:* Fax: +54 358 4676233 (G.M. Morales); fax: +34 915644853 (H.J. Salavagione).
E-mail addresses: gmorales@unrc.edu.ar (G.M. Morales), horacio@ictp.csic.es (H.J. Salavagione).
0008-6223/$ - see front matter © 2011 Elsevier Ltd. All rights reserved.
doi:10.1016/j.carbon.2011.03.008

Raman spectroscopy [14]. Liu et al. synthesized ionic-liquid-functionalized graphite sheets by applying 15 V between two graphite rods immersed in a water/ionic–liquid mixture [16], but the nature of the method produced graphene with high defect densities. In addition, Lu et al. reported the synthesis of fluorescent carbon nanostructures – including graphene – by using ionic liquid-assisted electrochemical exfoliation of graphite electrodes, also under oxidative conditions [17].

The exfoliation of graphite associated to the charging/discharging process is a well known phenomenon in the field of lithium-ion batteries using carbonaceous material. In fact, it is an undesired phenomena occurring during lithium intercalation/de-intercalation, leading to severe battery failure. In this context, much effort has been invested in engineering methods to avoid graphite exfoliation [18–20]. Under appropriate experimental conditions, graphite can be electrochemically oxidized and reduced to give C_n^+ and C_n^- lattices which can hold anions and cations respectively [21,22]. In addition, when a sufficiently negative (positive) potential is applied to a graphite-working electrode in aqueous solution, molecular hydrogen (O_2, CO_2 and GO) can be produced simultaneously to the intercalation process. To the best of our knowledge, the electrochemical production and subsequent intercalation of hydrogen on a graphite electrode coupled with the expansion and exfoliation assisted by hydrogen gas evolution has not been studied to date. Moreover, the electrochemical intercalation of anions – in this work, perchlorate – and posterior exfoliation of graphite in aqueous acid media has been investigated in more detail [23–28]. For example: (a) it has been shown that, the perchlorate ion is one of the best intercalating species at low acid concentrations [23] and (b) the anion intercalation can subsequently damage the sp^2 lattice due to side reactions such as GO and carbon dioxide (CO_2) formation [24,29]. However, by employing concentrated perchloric acid and with a careful selection of the intercalation potential, the contribution of those reactions, and consequently the creation of defects in the carbon network, can be minimized [26,28].

Here we report a simple method to produce FLG that combines the anodic and cathodic electrochemical intercalation of graphite in aqueous perchloric acid and posterior expansion by microwave radiation. This method has several advantages: First, strong oxidizing conditions are avoided, thus irreversible sp^3 defects caused under oxidation are not generated. Second, complex and expensive organic compounds are not necessary. Third, contaminants in the final product – hydrogen, protons, perchloric acid, perchlorate and water – can be eliminated by simple water-washing and further evaporation. Fourth, if some degree of functionalization – oxidation – is required, this can be tuned by choosing the appropriate potential and time applied during the electrochemical treatment.

2. Experimental

2.1. Electrochemical measurements

Electrochemical experiments were performed using a conventional one-compartment three-electrode electrochemical cell. The working electrode (WE) was a 1 mm thick laminated graphite foil of dimensions 8 mm × 15 mm (SIGRAFLEX®, Germany) , a normal hydrogen electrode (NHE) was employed as the reference electrode (RE), and in order to avoid contamination by metals, a piece of large surface area carbon [30] served as the counter electrode (CE). All experiments were conducted at room temperature 25 ± 2 °C using an AutoLab PGSTAT 12 potentiostat, controlled by GPES 4.9 electrochemical software (Eco-Chemie, Utrecht, The Netherlands). The potentials are expressed throughout with respect to the NHE.

2.2. Preparation of high quality FLG

The FLG was obtained by an electrochemical treatment followed by microwave-assisted thermal expansion and ultrasonic exfoliation of laminated graphite.

Electrochemical pre-expansion of a graphite electrode: The WEs were initially characterized by means of cyclic voltammetry (CV), and then subjected to double potential step experiments. A potential of 0 V was initially applied for 10 s, so it may be assumed that at zero time no faradaic reactions took place on the surface of the electrode. A perturbation potential was then imposed for the time period t, ranging from 0 to τ, and then the potential was reset to the original value for 10 s. The value of τ was typically 1200 s for cathodic potentials. However, positive potentials lead to electrode exfoliation after ca. 10 min and solids are observed at the bottom of the cell. During the perturbations the current was recorded as a function of time.

2.2.1. Preparation of EG

The second step involves thermal treatment assisted by microwave radiation. The electrochemically pre-expanded electrodes were immediately introduced into a conventional microwave oven (2.4 GHz) and treated for 5–10 s at a nominal power of 800 W under argon atmosphere.

2.2.2. Exfoliation of EG

Finally, the EG was dispersed into *N*-methyl-1-pyrrolidone (NMP) by treatment with an ultrasonic finger during five minutes. As has been demonstrated, the ultrasonic treatment is critical since it should be applied during a minimum period of time in order to ensure exfoliation but without exceeding the time in which irreversible damage is caused to the sp^2 network [31].

The product was centrifuged at 2000 rpm for 30 min and the precipitate was discarded to ensure that single or FLG was obtained.

2.3. Characterization of FLG

The actual concentration of the FLG solution was calculated as follows. After centrifugation 50 μL of graphene solution were transferred to a pre-weighted DSC crucible and dried under vacuum at 50 °C for 72 h. The crucible with the carbonaceous residue was weighed and the mass of graphene calculated by difference.

The EG samples were examined by scanning electron microscopy (SEM) employing a Philips XL30 SEM equipment operating at 25 kV.

High resolution transmission electron microscopy (HRTEM) was carried out in a Philips Tecnai 20F FEG microscope operating at 200 kV, equipped with a Scanning Transmission Electron Microscopy (STEM) module, with a dark field high angle annular detector for Z-contrast imaging. Crystal structure studies were carried out by electron diffraction pattern simulation, using Fast Fourier Transform (FFT) of the HRTEM images. For TEM measurements 5 μL of FLG dispersion in NMP were deposited onto the holey copper TEM grids by drop-casting and dried under vacuum.

UV/Vis absorption spectra of FLG dissolved in NMP were recorded on a Perkin Elmer Lambda 40 spectrophotometer.

The infrared spectra were recorded at 4 cm^{-1} resolution using a Perkin Elmer System 2000 FTIR spectrometer coupled to an i-Series IMAGE Infrared microscope equipped with a cooled HgCaTe detector. The samples were deposited on a Low-E slide (Keveley Technologies Inc., Chesterland, OH, USA) and recorded in reflection–absorption mode through a 100 μm aperture.

Confocal Raman measurements were made in the Raman Microspectroscopy Laboratory of the Characterization Service in the Institute of Polymer Science & Technology, CSIC. A Renishaw InVia Reflex Raman system (Renishaw plc., Wotton-under-Edge, UK) was used employing a grating spectrometer with a Peltier-cooled charge-coupled device (CCD) detector, coupled to a confocal microscope. All spectra were processed using Renishaw WiRE 3.2 software. The Raman scattering was excited using an Argon ion laser wavelength of 514.5 nm. The laser beam was focused on the sample with a 100× microscope objective (N.A. = 0.85), with a laser power at the sample of ⩽2 mW.

3. Results and discussion

As described before, we produced FLG in three steps: electrochemical treatment followed by microwave-assisted thermal expansion and ultrasonic exfoliation of laminated graphite. After the first two steps EG is obtained. The subsequent exfoliation of this EG gives the final FLG. We carefully studied the materials produced through the whole process of preparation.

Consider a graphite electrode subjected to a potential step from a non-faradaic region to a more negative potential. In the simplest scenario there are two different events that can contribute to the measured current: (a) charging of the electric double-layer and (b) faradaic process if the potential is low enough to produce a reduction on the electrode surface. Both are strongly dependent on the electrochemically active area presented by the electrode. In most of the electrochemical experiments the area of the electrode does not change throughout the experiment and the current–time response follows the Cottrell equation [32]. But in an intercalation experiment, the active area changes dramatically. Considering the cathodic and anodic intercalation in more detail:

Firstly, the potential of a graphite electrode in contact with an aqueous acid solution is stepped from 0 V to regions where atomic hydrogen is produced according to the reaction:

$$H_3O^{<}ce:sup>+</ce:sup>+e^- \rightarrow H + H_2O \quad (I)$$

The atomic hydrogen formed in (I) can recombine producing molecular hydrogen (II), or absorb on the carbon surface (III) and then either form molecular hydrogen via desorptive recombination (IV and V), or diffuse into the graphite host lattice [33]

$$2H \rightarrow H_2 \quad (II)$$

$$C_n + H \rightarrow C_nH_{ad} \quad (III)$$

$$C_nH_{ad} + H_2O + e^- \rightarrow H_2 + OH^- + C_n \quad (IV)$$

$$C_nH_{ad} + C_nH_{ad} \rightarrow H_2 + 2C_n \quad (V)$$

In a second experiment, the potential of the WE was also stepped to positive potentials where perchlorate ions are intercalated into the graphite according to the following reaction [24]:

$$C_n + A^- \rightarrow C_n^+A^- + e^- \quad (VI)$$

Concurrently to the intercalation process, faradaic reactions such as oxygen evolution and carbon oxidation to form GO and CO_2 are produced in aqueous acid solutions [21].

Fig. 1 shows typical chronoamperometric response curves to different potential steps applied to the WEs in 1 M $HClO_4$. In all cases, when a negative (positive) potential step is applied, the cathodic (anodic) current increases rapidly and then decreases for a short period of time to finally increase again gradually. The perturbation in the potential applied to the WE can produce different processes. Let us analyze the cathodic intercalation first. The quick initial increase of the current can be ascribed to the double-layer charging of the pristine graphite electrode. The subsequent response in current is dominated by reaction (I). In this stage of the treatment, the current diminishes – clearly visible when 0 → −1.5 V (Fig. 1, curve a) and 0 → +1.7 V (Fig 1, curve e) are applied to the electrode – according to a Cottrell-like behavior characteristic of an electrochemical process limited by diffusion. However, deviations – the current dependence is not linear with $t^{1/2}$ – become more important as time increases. Therefore processes other than faradaic ones should be occurring simultaneously. As discussed above, the molecular hydrogen formed in (I) can diffuse into the graphite producing hydrogen intercalation and consequently expansion of the WE. Indeed, the

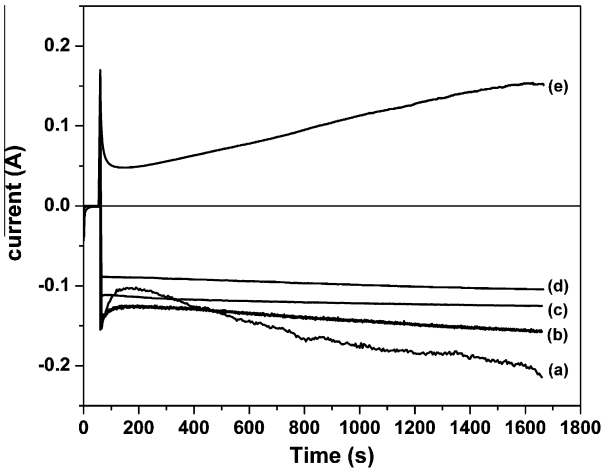

Fig. 1 – Potential-step chronoamperograms of a laminated graphite electrode in 1 M $HClO_4$. The potential was stepped from 0 to −1.5 V (a), −1 V (b), −0.8 V (c), −0.6 V (d) and +1.7 V (e).

expansion phenomena in the WE can be observed in the electrochemical cell by the naked eye. The WE expansion increases the electrochemically active area with a simultaneous rise in the current mainly due to the faradaic reaction (I). This process becomes more important with time and explains both the deviation from the Cottrell equation and the final current rise observed in the chronoamperometric curves. It should be mentioned that no significant expansion of the graphite electrode was observed for potentials in the range of 0 to −0.6 V. The over-potential for the reduction of hydrogen ions on graphite in acid media obtained from CV experiments is roughly −0.5 V. Thus it can be concluded that reaction (I) is necessary for the expansion process, even when the molecular hydrogen evolution through the Tafel reaction (V) is the favored step after the formation of atomic hydrogen in acidic medium [31]. This fact is in good agreement with previous observations of hydrogen insertion into carbon fabric in aqueous H_2SO_4 [34].

Hydrogen evolution plays an important function in the expansion mechanism. This fact could be explained by a similar mechanism to the exfoliation of graphite by electrochemical decomposition of propylene carbonate [35]. The electrolyte penetrates into graphite openings such as pores and defects. Then, a proton is reduced inside those openings to hydrogen which can produce hydrogen gas (reactions I and II). The large amount of molecular hydrogen produced in a short time induces mechanical stress in the interface of the carbon/electrolyte solution helping to overcome the van der Waals forces between graphene layers. Hydrogen evolution is more pronounced as the cathodic potential becomes larger. In fact, negative potentials greater than −1.7 V result in exfoliation of graphite particles which are deposited on the bottom of the cell. In addition, fluctuation in the current observed in the chronoamperograms in Fig. 1a and b are attributed to perturbations of the WE surface produced by the violent hydrogen bubbling. A quantitative interpretation of the chronoamperometric curves can be performed using a model of nucleation and growth plus a moving boundary as was recently reported by Levi et al. for the electrochemical intercalation of lithium in graphite [36]. While qualitatively such model seems to be operative, such analysis is out of the scope of the present work and will be reported elsewhere. A similar behavior is observed for positive potential steps, in agreement with the nucleation and growth mechanism proposed by Bard et al. for the oxidation of graphite [37]. For comparison purposes, Fig. 1 shows the $0 \rightarrow +1.7$ V step since potentials above +2 V produce exfoliation of the graphite WE in a few minutes, probably due to a combination of GO formation and CO_2 and O_2 evolution.

The EG obtained after electrochemical intercalation/microwave expansion was characterized by SEM and Raman spectroscopy. Optical inspection suggests that the volume of the EG increases as the potential modulus increases (Supporting Information, Fig. S1). The volume depends on the polarity of the electrode, revealing a higher expansion for positively-polarized electrodes (Fig. S1). Nevertheless, in order to prevent the formation of oxygenated groups that can lead to sp^3 carbon and breaking the sp^2 network, the cathodic potentials are more appropriate, producing the most favorable result when −1 V is applied to the WE.

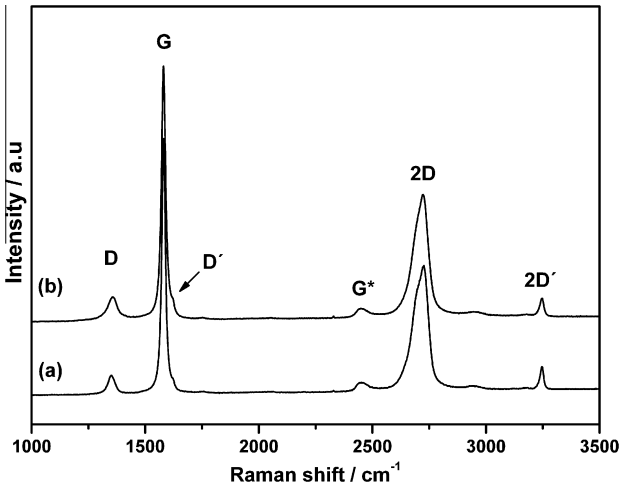

Fig. 2 – Raman spectra of (a) laminated graphite and (b) EG prepared by electrochemical treatment at −1 V with band assignments given.

The morphological characterization of the EG shows the typical worm-like shape of the EG with thin layered graphene structures (Fig. S2) [12]. Figure S2b indicates the presence of layered graphene structures. All the EGs produced in this work display similar features. The stacked graphene laminates appear wrinkled, which is typical of graphene sheets [38]. These observations suggest that the EG obtained by our method are similar to those obtained by using other procedures.

This EG has also been characterized by Raman spectroscopy (Fig. 2). The most important features in the Raman spectra obtained using a laser excitation of 514.5 nm are the G band appearing around 1580 cm^{-1}, the second order 2D band at around 2700 cm^{-1} and the disorder-induced D and D′ bands at 1350 cm^{-1} and 1620 cm^{-1}, respectively. The second order 2D′ mode can also be observed close to 3250 cm^{-1}. The Raman spectra in Fig. 2 compare the initial graphite and EG prepared using a perturbation potential of −1.0 V. The first-order G-mode appears in both samples at 1581 cm^{-1}, whereas in the D-mode for the EG, FWHM broadening from 35 to 45 cm^{-1} and slight shift in peak frequency from 1350 to 1356 cm^{-1} was observed. Evidence for the D′ band at around 1622 cm^{-1} is also present in both spectra. However, the pre-treatment does not appear to have a negative influence on the material integrity. In fact, the I_D/I_G ratio, which is a measure of the defects in the carbon network, remains practically constant during the entire process. From the Raman spectroscopy data, it can be concluded that the electrochemical treatment and the thermal expansion are not detrimental to the sp^2 structure of graphite.

FLG have been obtained by ultrasonic treatment of EG in NMP during five minutes. After centrifugation, well-dispersed graphene solutions are obtained (Fig. 3). The concentration of graphene produced from negatively polarized electrodes, lies in the order of 0.6–0.8 g L^{-1} for samples prepared at −1 V. However, higher values can be obtained depending on the electrochemical conditions (Table S1). Beyond the experimental uncertainties and the possibility that some NMP can be irreversibly adsorbed on the graphene layers, the graphene

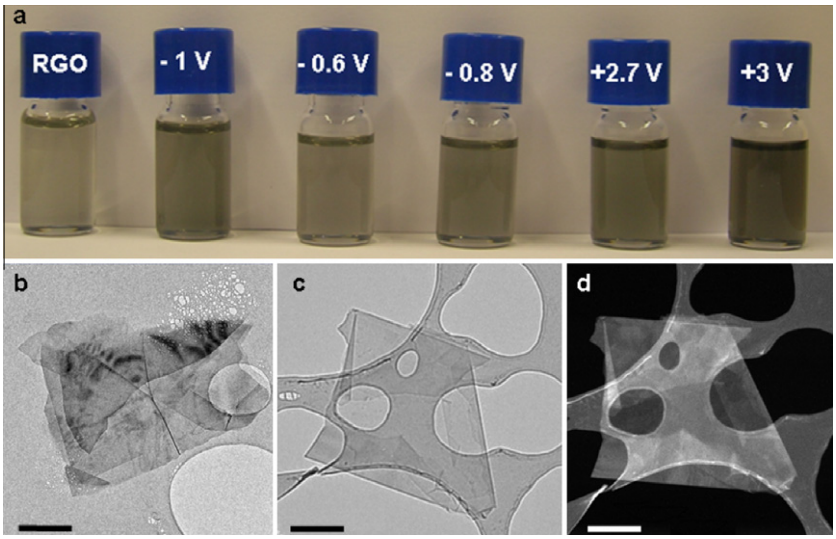

Fig. 3 – (a) Stable dispersions of FLG prepared at different applied potentials in NMP (potential values in the figure). The dispersion of reduced graphite oxide (RGO) in NMP is shown for comparison. (b) and (c) Bright field micrographs of a graphene flake, in (c) the image is intentionally out of focus to increase the contrast. (d) Z-contrast dark field image, higher intensity indicates higher thickness. Scale bars: 1 μm.

concentration obtained by our method is somewhat higher than the obtained by other procedures (~0.01–0.03 g L^{-1}) [39,40] and similar to values recently reported by Coleman and co-workers (up to 1.2 g L^{-1}) employing much longer procedures such as ultrasonic treatment for more than 400 h [31]. This level of concentration has only been achieved by reduction of GO whose properties, due to sp^3 defects in the carbon lattice, are very poor compared with defect-free graphene obtained here. In addition, our method produces FLG with higher lateral dimensions and better quality (lower degree of structural defects) than graphene obtained by exhaustive ultrasonic treatment [31], as will be discussed later.

The absorption spectra of the FLG dispersions in NMP are flat and featureless in the visible region (Fig. S3) as expected for quasi two-dimensional materials [39]. In addition, the observed low scattering effect is indicative of a dispersion containing non-aggregated ultrathin nanostructures. Also the infrared spectrum of FLG, obtained by reflection–absorption mode on a glass slide, shows no features in the carbonyl or hydroxyl regions (Fig. S4) suggesting that no defects has been created during the preparation procedure. The typical bands for GO around 3600–3000 cm^{-1} (ν_{OH}), 1715 cm^{-1} ($\nu_{C=O}$), 1616 cm^{-1} (β_{OH}) and 1368 cm^{-1} (β_{OH}), are not present and the spectrum of FLG obtained at a polarization of −1 V resembles that of graphite where only the bands of skeletal vibrations of graphitic domains are observed at 1550 cm^{-1} ($\nu_{C=C}$) and 1025 cm^{-1} (ν_{C-C}) (Fig. S4).

The level of exfoliation, lateral size, thickness and the structure of the material dispersed can be analyzed by TEM by dropping a small quantity of the dispersion onto a holey carbon grid (Fig. 3). Fig. 3b and c show bright field images of the typical flakes observed; the image of Fig. 3c is intentionally out of focus to show the presence of folded layer and multilayer graphene. The lateral size of the flakes is around a few micrometers, which is somewhat larger than that reported for exfoliation of graphite in NMP by sonication [31,39]. Fig. 3d is the Z-contrast image corresponding to Fig. 3c. Even in the thinner areas of the flakes it was possible to observe the presence of several layers of graphene. It should be emphasized that, even if they are present in the sample, single layers are difficult observe in a TEM experiment because of the high tendency to stacking during drying on the TEM grid. Two examples are shown in Fig. 4. In Fig. 4a, 10 graphite layers are observed, whereas in Fig. 4b the fast Fourier transform (FFT) pattern simulation (inset) indicates the superposition of two hexagonal structures rotated 30°. Regarding the quality of the graphene sheets, the majority of the flakes showed intermixing of defaulted and ordered areas [41]. Image filtering of both defaulted and undefaulted areas is shown in Fig. 4c.

Even if it were possible, it is not obvious that the defects were generated during the expansion–exfoliation procedure. In fact, the graphite electrode used as starting material contains some structural defects as was observed from the Raman spectrum in Fig. 2. However, it cannot be ignored that the defects may have their origin in different steps of the synthetic (i.e. edge defects produced during the intercalation or exfoliation) or the characterization process (i.e. damage caused by the electron beam during the acquisition of images) [42].

Due to the lack in uniformity it is not clear that the intensity of the {2 1 1 0} and {1 1 0 0} reflections can be used in this case as a fingerprint to indicate the presence of graphene monolayers. The high resolution image of Fig. 4c is representative of the images obtained from the thinner flakes. As a consequence of the non-homogeneous sample, different intensities of the spots associated with the structural misorientations can be observed in the Fourier transform pattern (ftp) diffraction simulation. The thickness of the imaged area in Fig. 4c is well below four monolayers, observed at the edge, as indicated by the difference in intensity obtained at the STEM-Z contrast images.

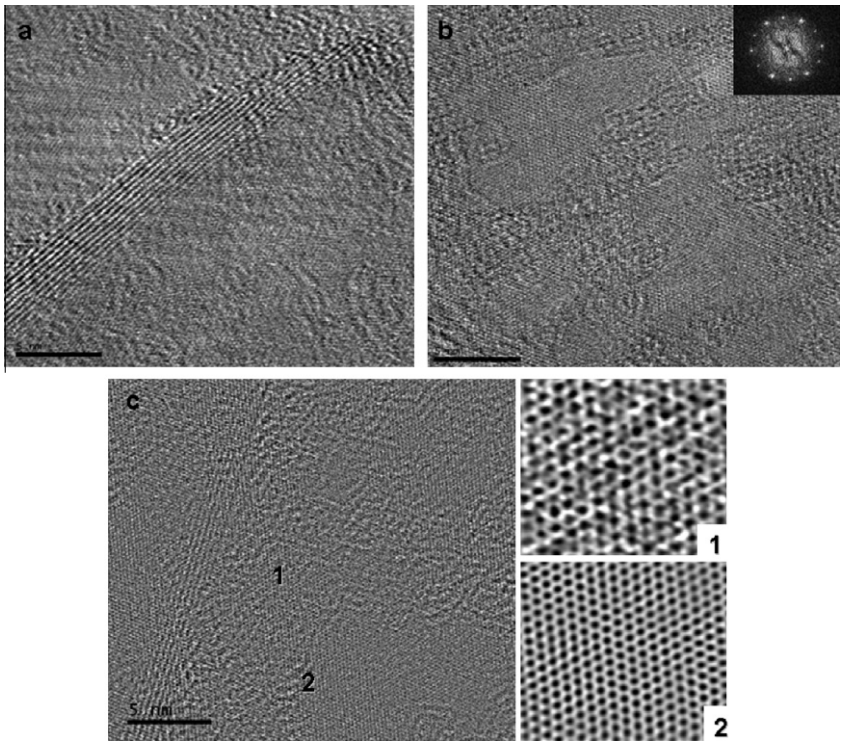

Fig. 4 – (a) and (b) HRTEM micrographs of stacked flakes: (a) fringes at the edge of a flake, indicating the stacking of 10 monolayers, (b) Image and FFT electron diffraction pattern simulation at the inset, where the superposition of two hexagonal structures rotated 30° is observed; (c) the fringes indicate a maximum stacking of four monolayers (left). The filtered images make on the same conditions of two contiguous areas with thickness well below four monolayers are also shown (right): top correspond to defaulted and bottom to free of defects areas. Scale bars: 5 nm.

In order to obtain more evidence on the average number of graphene layers and the quality of the samples after exfoliation, Raman spectra of the FLG samples were recorded after deposition from solution onto quartz microscope slides. The I_D/I_G ratio maintains the values observed prior to the exfoliation step, and the low intensity of the D band and the lack of a substantial D′ band indicate that high quality FLG is obtained (Fig. 5a), different to that found for graph-

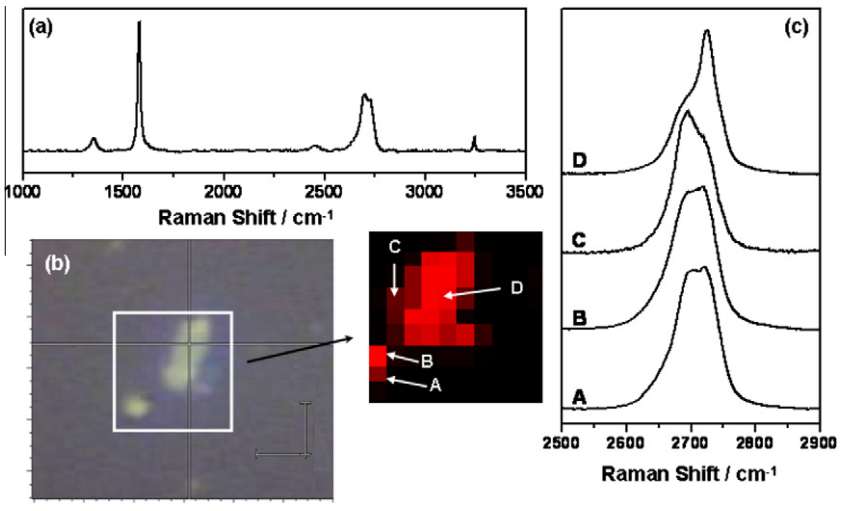

Fig. 5 – (a) Raman spectrum observed from exfoliated −1 V FLG sample deposited on a quartz slide, (b) optical image of a typical deposit on the quartz slide and false-color map of the zone indicated, and (c) representative spectra from the points indicated of the 2D region of FLG. Scale bars in b: 2 m.

ene prepared by sonication of graphite over long periods of time [31]. These results are reasonable since the electrochemical pre-treatment diminishes the cohesive forces between graphene laminates, and consequently shorter sonication times are required, and less defective materials produced. These results also suggest that the defects viewed in TEM images can be associated to irregularities in the edge plane.

On the other hand, although the efficiency of intercalation/expansion is higher for positive potentials due to intercalation of more voluminous perchlorate ions (Fig. S1), oxidative potentials over reasonable times lead to side reactions forming GO and CO_2 damaging in sp^2 network [24,29] . Therefore, cathodic potentials were chosen to preserve the sp^2 network and the outstanding properties of graphene. To ensure high intercalation avoiding the formation of sp^3 defects during anodic treatment, a lower positive potential or shorter times should be employed. Further study and optimization of the process is currently underway in our laboratory.

Characteristic spectra of multiple and FLG were observed, as could be determined by the analysis of the second order 2D peaks arising from the zone boundary phonons [43]. As an example, Fig. 5b shows an image of a graphene deposit observed on the quartz slide of the same sample, and a false color image of the baseline to 2680 cm^{-1} intensity, where the darker squares represent higher intensity. Fig. 5c presents the Raman spectra observed at different points marked on the sample in the high frequency region corresponding to the 2D modes. Spectra at points A–C correspond to FLG of 3–6 layers [44–46] whilst the spectrum at point D coincides with the thicker area at the centre of the deposit and corresponds more closely to that of graphite. Raman and TEM results suggest the formation of polydisperse samples composed of tri, four, few and multilayer graphene. Obviously, the method here reported can be optimized to obtain less polydisperse products and single layer graphene [47,48]. However; here our objective was to show that the electrochemical intercalation of graphite in acid media is an interesting alternative to produce FLG combining large quantity, high quality and short time.

4. Conclusions

In summary, a new method to produce FLG has been described. The GIC are synthesized in aqueous perchloric acid under well-defined electrochemical-potential control. Further thermal expansion and the subsequent exfoliation by ultrasound yield a material composed mainly of FLG. The spectroscopic and morphologic characterization of the final material shows that by selecting the appropriated conditions the synthetic procedure does not produce damage to the sp^2 carbon lattice. This work demonstrates the potential of electrochemistry to produce GIC as precursor to a synthesize FLG with different degrees of chemical modification.

5. Electronic Supplementary Information

Optical images of the WEs treated at different potentials, UV–visible and FTIR characterization SEM images of EG, and table of disperssability of FLG as a function of the applied potentials.

Acknowledgment

Financial support from the Spanish Ministry of Science and Innovation (MICINN) (MAT2009-09335 and MAT-2007-66181) and Argentine Ministry of Science, Technology and Productive Innovation (FONCYT PICT 04 25521, PAE 04 22771 and PICT 07 02214) are grateful acknowledged. H.J. Salavagione thanks MICINN by a Ramón y Cajal research position. G.M. Morales and C.A. Barbero are permanent research fellows of CONICET. TEM work has been carried out at LABMET (Red de Laboratorios de la Comunidad de Madrid). The help of M.I. Ortiz with the TEM is acknowledged.

REFERENCES

[1] Geim AK, Novoselov KS. The Rise of Graphene. Nat Mater 2007;6(3):183–91.
[2] Novoselov KS, Geim AK, Morozov SV, Jiang D, Zhang Y, Dubonos SV, et al. Electric field effect in atomically thin carbon films. Science 2004;306(5696):666–9.
[3] Novoselov KS, Jiang Z, Zhang Y, Morozov SV, Stormer HL, Zeitler U, et al. Room-temperature quantum Hall effect in graphene. Science 2007;315(5817):1379.
[4] Novoselov KS, McCann E, Morozov SV, Fal'ko VI, Katsnelson MI, Zeitler U, et al. Unconventional quantum Hall effect and Berry's phase of 2π bilayer graphene. Nat Phys 2006;2(3):177–80.
[5] Zhang Y, Tan Y-W, Stormer HL, Kim P. Experimental observation of the quantum Hall effect and Berry's phase in graphene. Nature 2005;438(7065):201–4.
[6] Novoselov KS, Geim AK, Morozov SV, Jiang D, Katsnelson MI, Grigorieva IV, et al. Two-dimensional gas of massless Dirac fermions in graphene. Nature 2005;438(7065):197–200.
[7] Bolotin KI, Sikes KJ, Jiang Z, Klima M, Fudenberg G, Hone J, et al. Ultrahigh electron mobility in suspended graphene. Solid State Commun 2008;146(9–10):351–5.
[8] Stoller MD, Park S, Zhu Y, An J, Ruoff RS. Graphene-based ultracapacitors. Nano Lett 2008;8(10):3498–502.
[9] Allen MJ, Tung VC, Kaner RB. Honeycomb carbon: a review of graphene. Chem Rev 2010;110(1):132–45.
[10] Chung DDL. Exfoliation of graphite. J Mater Sci 1987;22(12):4190–8.
[11] Chung DDL. Review graphite. J Mater Sci 2002;37(8):1475–89.
[12] Stankovich S, Dikin DA, Piner RD, Kohlhaas KA, Kleinhammes A, Jia Y, et al. Synthesis of graphene-based nanosheets via chemical reduction of exfoliated graphite oxide. Carbon 2007;45(7):1558–65.
[13] Viculis LM, Mack JJ, Mayer OM, Hahn HT, Kaner RB. Intercalation and exfoliation routes to graphite nanoplatelets. J Mater Chem 2005;15(9):974–8.
[14] Guo HL, Wang XF, Qian QY, Wang FB, Xia XH. A green approach to the synthesis of graphene nanosheets. ACS Nano 2009;3(9):2653–9.
[15] Shao Y, Wang J, Engelhard M, Wang C, Lin Y. Facile and controllable electrochemical reduction of graphene oxide and its applications. J Mater Chem 2010;20(4):743–8.
[16] Liu N, Luo F, Wu H, Liu Y, Zhang C, Chen J. One-step ionic-liquid-assisted electrochemical synthesis of ionic-liquid-functionalized graphene sheets directly from graphite. Adv Funct Mater 2008;18(10):1518–25.

[17] Lu J, Yang JX, Wang J, Lim A, Wang S, Loh KP. One-pot synthesis of fluorescent carbon nanoribbons, nanoparticles, and graphene by the exfoliation of graphite in ionic liquids. ACS Nano 2009;3(8):2367–75.
[18] Wu YP, Rahm E, Holze R. Carbon anode materials for lithium ion batteries. J Power Sources 2003;114(2):228–36.
[19] Campana FP, Buqa H, Novák P, Kötz R, Siegenthaler H. In situ atomic force microscopy study of exfoliation phenomena on graphite basal planes. Electrochem Commun 2008;10(10):1590–3.
[20] Märkle W, Tran N, Goers D, Spahr ME, Novák P. The influence of electrolyte and graphite type on the PF_6^- intercalation behaviour at high potentials. Carbon 2009;47(11):2727–32.
[21] Besenhard JO, Möhwald H, Nickl JJ. Preparation and characterization of graphite compounds by electrochemical techniques. Synth Met 1981;3(3–4):187–94.
[22] Noel M, Santhanam R. Electrochemistry of graphite intercalation compounds. J. Power Sources 1998;72(1):53–65.
[23] Beck F, Junge H, Krohn H. Graphite intercalation compounds as positive electrodes in galvanic cells. Electrochim Acta 1981;26(7):799–809.
[24] Alsmeyer DC, McCreery RL. In situ Raman monitoring of electrochemical graphite intercalation and lattice damage in mild aqueous acids. Anal Chem 1992;64(14):1528–33.
[25] Goss CA, Brumfield JC, Irene EA, Murray RW. Imaging the incipient electrochemical oxidation of highly oriented pyrolytic graphite. Anal Chem 1993;65(10):1378–89.
[26] Zhang J, Wang E. STM investigation of HOPG superperiodic features caused by electrochemical pretreatment. J Electroanal Chem 1995;399(1–2):83–9.
[27] Alliata D, Häring P, Haas O, Kötz R, Siegenthaler H. Anion intercalation into highly oriented pyrolytic graphite studied by electrochemical atomic force microscopy. Electrochem Commun. 1999;1(1):5–9.
[28] Schnyder B, Alliata D, Kötz R, Siegenthaler H. Electrochemical intercalation of perchlorate ions in HOPG: an SFM/LFM and XPS study. Appl Surf Sci 2001;173(3–4):221–32.
[29] Kötz R, Barbero C, Schnyder B, Haas O. Spectroscopic ellipsometry of carbon electrodes during electrochemical activation. Thin Solid Films 1993;233(1–2):69–73.
[30] Bruno MM, Cotella NG, Miras MC, Koch T, Seidler S, Barbero C. Characterization of monolithic porous carbon prepared from resorcinol/formaldehyde gels with cationic surfactant. Colloid Surf A 2010;358(1–3):13–20.
[31] Khan U, O'Neill A, Lotya M, De S, Coleman JN. High-concentration solvent exfoliation of graphene. Small 2010;6(7):864–71.
[32] Bard AJ, Faulkner LR. Electrochemical methods: fundamentals and applications. 2nd ed. New York: Wiley; 2001.
[33] Bockris JOM, Reddy AKN. Modern electrochemistry, vol. 2. New York: Plenum Press; 1970.
[34] Jurewicz K, Frackowiak E, Béguin F. Towards the mechanism of electrochemical hydrogen storage in nanostructured carbon materials. Appl Phys A – Mater 2004;78(7):981–7.
[35] Winter M, Moeller KC, Besenhard JO. In: Nazri G-A, Pistoa G, editors. Carbonaceous and graphitic anodes in Lithium batteries: science and technology. Boston, Dordrecht, New York, London: Kluwer Academic Publishers; 2004.
[36] Levi MD, Markevich E, Wang C, Aurbach D. Chronoamperometric measurements and modeling of nucleation and growth, and moving boundary stages during electrochemical lithiation of graphite electrode. J Electroanal Chem 2007;600(1):13–22.
[37] Gewirth AA, Bard AJ. In situ scanning tunneling microscopy of the anodic oxidation of highly oriented pyrolytic graphite surfaces. J Phys Chem 1988;92(20):5563–6.
[38] Meyer JC, Geim AK, Kaysnelson MI, Novoselov KS, Booth TJ, Roth S. The structure of suspended graphene sheets. Nature 2006;446(7131):60–3.
[39] Hernandez Y, Nicolosi V, Lotya M, Blighe FM, Sun Z, De S, et al. High-yield production of graphene by liquid-phase exfoliation of graphite. Nat Nanotechnol 2008;3(9):563–8.
[40] Hamilton CE, Lomeda JR, Sun Z, Tour JM, Barron AR. High-yield organic dispersions of unfunctionalized graphene. Nano Lett 2009;9(10):3460–2.
[41] Gómez-Navarro C, Meyer JC, Sundaram RS, Chuvilin A, Kurasch S, Burghard M, et al. Atomic structure of reduced graphene oxide. Nano Lett 2010;10(4):1144–8.
[42] Hashimoto A, Suenaga K, Gloter A, Urita K, Iijima S. Direct evidence for atomic defects in graphene layers. Nature 2004;430(7002):870–3.
[43] Ferrari AC, Meyer JC, Scardaci V, Casiraghi C, Lazzeri M, Mauri F, et al. Raman spectrum of graphene and graphene layers. Phys Rev Lett 2006;97(18):187401.
[44] Ferrari AC. Disorder, electron–phonon coupling, doping and nonadiabatic effects. Solid State Commun 2007;143(1–2):47–57.
[45] Dresselhaus MS, Jorio A, Hofmann M, Dresselhaus G, Saito R. Perspectives on carbon nanotubes and graphene raman spectroscopy. Nano Lett 2010;10(3):751–8.
[46] Hao Y, Wang Y, Wang L, Ni Z, Wang Z, Wang R, et al. Probing layer number and stacking order of few-layer graphene by Raman spectroscopy. Small 2010;6(2):195–200.
[47] Green AA, Hersam MC. Solution phase production of graphene with controlled thickness via density differentiation. Nano Lett 2009;9(12):4031–6.
[48] Green AA, Hersam MC. Emerging methods for producing monodisperse graphene dispersions. J Phys Chem Lett 2010;1(2):544–9.